Journal of Materials Chemistry A

COMMUNICATION

View Article Online
View Journal | View Issue

Cite this: J. Mater. Chem. A, 2014, 2, 10370

Received 7th March 2014
Accepted 28th April 2014

DOI: 10.1039/c4ta01152j

www.rsc.org/MaterialsA

Self-powered electrochemical deposition of Cu@Ni(OH)$_2$ nanobelts for high performance pseudocapacitors†

I-Chun Chang,[a] Ting-Ting Chen,[a] Min-Han Yang,[a] Hsin-Tien Chiu[b] and Chi-Young Lee*[a]

Two aluminum-driven spontaneous electrochemical reactions are developed for depositing Cu@Ni(OH)$_2$ nanobelts on carbon/aluminum electrodes. The Cu@Ni(OH)$_2$ NBs function as pseudocapacitor electrodes, which exhibit a high specific capacitance of 2426 F g^{-1} and a remarkable rate performance.

Pseudocapacitors are attracting considerable interest, because of their high capacitance, rapid recharging and high power density, which overcome the limitations of conventional batteries and capacitors in electrochemical reactions.[1,2] As is widely known, transition metal oxides[3–8] and hydroxides,[9–12] as well as electronically conducting polymers[13,14] with multiple oxidation states, resulting in rich redox reactions, are ideal electrode materials used in pseudocapacitors. Nickel hydroxide (Ni(OH)$_2$) is an extensively used material for storing energy, because of its abundance, low cost, and high theoretical specific capacitance.[10–12] However, its insufficient electrical conductivity and short cycle life severely limit its usefulness.[15] Coating Ni(OH)$_2$ onto three dimensional (3D) conductive substrates shortens the electron transport distance[11,12] and substitutes some cations (such as Co) for Ni, substantially improving the rate capability and cycleablity.[16,17] However, substrate preparation and the subsequent Ni(OH)$_2$ decoration are typically complex and consume much energy. Owing to the global energy crisis, a simple and environmentally friendly means of fabricating high-performance electrodes is sought urgently.

Generally known as immersion plating, galvanic displacement is superior to high temperature processes in many ways, including the relative simplicity of the procedure, the inexpensive equipment required and the low operating temperature.[18–21] Unlike electrodeposition, galvanic displacement does not require an external power supply, but is driven by spontaneous dissolution of the sacrificial metal anode, which is accompanied by a reduction of coupled metal ions on the surface of the anode. However, galvanic displacement is frequently performed to synthesize hollow nanomaterials because the core anode typically functions as a sacrificial template or is encapsulated in a coating shell, limiting its reuse.[21–23] Our recent work presented the efficient growth of copper nanobelts (NBs) and nanorods on a conducting substrate by the surfactant-assisted galvanic displacement of Al.[18,19] Copper tends to grow on the connected conducting substrate rather than on Al foil itself in a normal galvanic displacement. This tendency can be exploited to coat Ni(OH)$_2$ on CuNBs through a further electrochemical reaction of the uncovered Al.

This work develops a two-step aluminum-driven spontaneous electrochemical deposition method, which includes the growth by galvanic displacement of a core of copper nanobelts (CuNBs) and the subsequent precipitation of a shell of Ni(OH)$_2$ nanosheets on the CuNBs. The proposed method is characterized by a relatively simple soaking process without the need for a power supply, as well as the formation of highly conductive 3D CuNBs interlacing networks that function as an excellent current collector. To the best of our knowledge, this work is the first to form a core–shell structure *via* two electrochemical reaction of the sacrificial Al anode. Importantly, the proposed method is scalable and conducive to mass production. The Cu@Ni(OH)$_2$ NB electrodes herein exhibit an excellent specific capacitance and remarkable rate capability. Moreover, the rate performance and capacitance retention are further improved by partially substituting Ni with Co.

Cu@Ni(OH)$_2$ NBs on the C/Al substrate were synthesized by a unique two-step spontaneous electrochemical deposition procedure, which is schematically depicted in Fig. 1. The procedure includes (a) the galvanic deposition of CuNBs on the carbon side of the C/Al substrate by immersing it into an aqueous solution of $CuCl_2$, CTAC and HNO_3 and (b) the coating of Ni(OH)$_2$ nanosheets onto the surfaces of CuNBs by further

[a]Department of Materials Science and Engineering, National Tsing Hua University Hsinchu, Taiwan 30043, Republic of China. E-mail: cylee@mx.nthu.edu.tw
[b]A Department of Applied Chemistry, National Chiao Tung University Hsinchu, Taiwan 30050, Republic of China. E-mail: htchiu@faculty.nctu.edu.tw

† Electronic supplementary information (ESI) available: Experimental details, SEM, EDS, ICP, and TEM results. See DOI: 10.1039/c4ta01152j

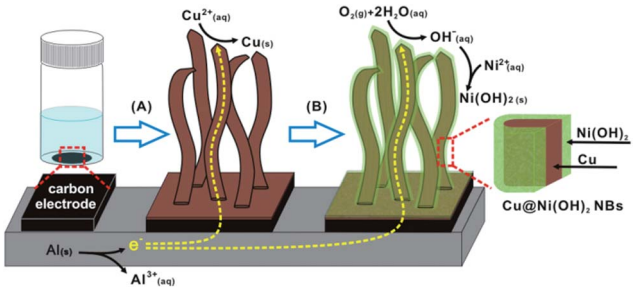

Fig. 1 Fabrication of $Cu@Ni(OH)_2$ nanobelts on carbon/aluminium.

immersing them into aqueous $NiSO_4$. In this two-step deposition process, Al foil has a critical role in both steps. The growth of CuNBs is based on a galvanic reduction of Cu and Al, which occurred spontaneously herein, because of the positive redox potential between Cu^{2+} and Al (eqn (1)). A previous study proposed the growth pathway for CuNBs.[18] Tiny hydrogen gaseous bubbles were also detected after 18 h and adsorbed on the surface of Al foil (eqn (2)). $Ni(OH)_2$ nanosheets precipitated on CuNBs in an aqueous solution of $NiSO_4$, owing to a local increase in the pH by a redox reaction between oxygen and Al (eqn (3) and (4)).

$$3Cu^{2+}(aq) + 2Al(s) \rightarrow 3Cu(s) + 2Al^{3+}(aq),\ E^\circ = 2.00\ V \quad (1)$$

$$6H^+(aq) + 2Al(s) \rightarrow 3H_2(g) + 2Al^{3+}(aq),\ E^\circ = 1.66\ V \quad (2)$$

$$3O_2(g) + 6H_2O + 4Al(s) \rightarrow 12OH^-(aq) + 4Al^{3+},\ E^\circ = 2.04\ V \quad (3)$$

$$Ni^{2+}(aq) + 2OH^-(aq) \rightarrow Ni(OH)_2(s) \quad (4)$$

The phase structure of the CuNBs on the C/Al substrate is determined using X-ray diffraction (XRD) (Fig. S1†). The XRD reflection pattern demonstrates that the NBs comprise face-centered cubic (fcc) Cu (JCPDS 89-2838). The constant peak position indicates that the $Ni(OH)_2$ coating process does not change the phase structure of CuNBs. No peak of $Ni(OH)_2$ is obtained, probably because of the insufficient crystallinity of $Ni(OH)_2$ that was deposited on the surface of the CuNBs.

Fig. 2a displays the full-range X-ray photoelectron spectra (XPS). The pristine CuNBs yield two strong peaks and no satellite peak for cupric oxide (CuO) is obtained (Fig. 2b). The peaks at 932.4 and 952.2 eV that are associated with Cu $2p_{3/2}$ and Cu $2p_{1/2}$ photoelectrons may be attributed to metal Cu or cuprous oxide (Cu_2O) because of their very close binding energies.[24] Based on our previous investigation, transmission electron microscopic (TEM) analysis suggested the presence of a minute quantity of Cu_2O on the surface of the CuNBs.[18] In Fig. 2c, two oxygen bonds are seen in the O 1s spectrum: O1 at 531.2 eV is associated with nickel–oxygen bonds and O2 at 533.9 eV is associated with the oxygen in the physi- and chemisorbed water.[25] Fig. 2d displays the Ni 2p XPS spectrum, in which the typical Ni^{2+} $2p_{3/2}$ and $2p_{1/2}$ peaks with two shakeup satellites (denoted as "Sat.") are observed at 855.9 and 873.4 eV,[25] respectively. Characteristic of an $Ni(OH)_2$ phase, the

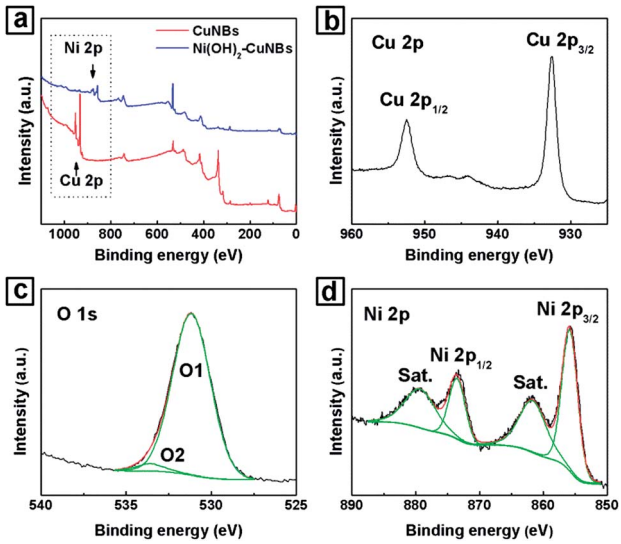

Fig. 2 (a) XPS survey of CuNBs and $Cu@Ni(OH)_2$ NBs, (b) XPS peaks of Cu 2p of pristine CuNBs, (c) XPS peaks of Ni 2p of $Cu@Ni(OH)_2$ NBs, and (d) XPS peaks of O 1s of $Cu@Ni(OH)_2$ NBs.

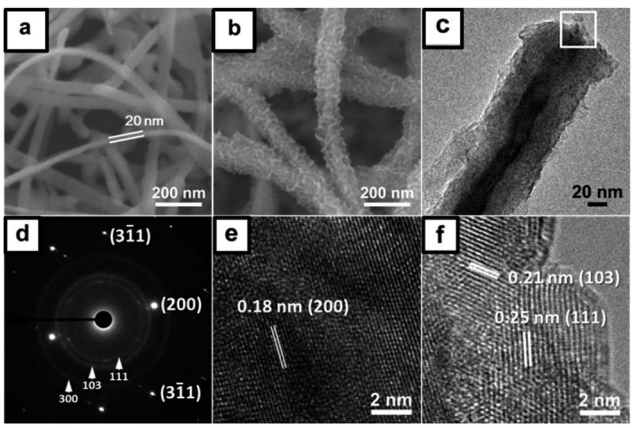

Fig. 3 SEM images of CuNBs (a) and $Cu@Ni(OH)_2$ NBs (b); TEM images (c) and SAED patterns (d) of $Cu@Ni(OH)_2$ NBs; high-resolution TEM (HRTEM) images of the Cu core (e) and the $Ni(OH)_2$ shell (f).

spin energy separation of 17.5 eV is consistent with previously reported data concerning Ni $2p_{3/2}$ and Ni $2p_{1/2}$ in $Ni(OH)_2$.[10,11]

Fig. 3 displays the field-emission scanning electron microscopic (SEM) and TEM images of the as-prepared samples. Fig. 3a presents the pristine CuNBs that are several tens of μm long and ~20 nm thick. The CuNBs grew densely and covered the carbon electrode surface, ultimately forming an interlacing network (Fig. S2a†). An energy-dispersive spectrum (EDS) demonstrates that the NBs comprise mostly Cu (Fig. S2b†). The Cl signal arises from the adsorption of CTAC on CuNBs and the carbon electrode. Fig. 3b presents the SEM images of samples following the deposition of $Ni(OH)_2$. The belt-like morphology is retained and the $Ni(OH)_2$ nanosheets are uniformly coated on the surface of the CuNBs. EDS analysis confirms that the core–shell NBs comprise Cu, Ni and O (Fig. S3a†). Fig. S3b† plots the relative mass of $Ni(OH)_2$ that is loaded on the CuNBs as a

function of time, determined from the difference between the $NiSO_4$ concentrations before and after coating with $Ni(OH)_2$ by inductively coupled plasma (ICP).

The structure and crystallinity of $Cu@Ni(OH)_2$ NBs are more closely characterized by TEM. Fig. 3c presents a low-magnification bright-field image of $Cu@Ni(OH)_2$ NBs. The surface of CuNBs is entirely covered by $Ni(OH)_2$ nanosheets with a thickness of ~20 nm (Fig. S4†). Fig. 3d presents the corresponding selected area electron diffraction (SAED) pattern, which includes both strong spots and week rings. The *d*-spacing, estimated from the spots that are closest to the center of the beam, is 0.18 nm, which is the *d*-spacing of Cu (200) planes (JCPDF 89-2838). The lattice parameter *a* is thus determined to be 0.36 nm, which is similar to the previously reported value for fcc Cu. From the above patterns, the crystallographic zone axis is [001]. The *d*-spacings from the rings are 0.25, 0.22 and 0.16 nm, which are consistent with the (111), (103) and (300) planes of α-$3Ni(OH)_2 \cdot 2H_2O$ (JCPDS 22-0444), indicating the formation of a polycrystalline α-$Ni(OH)_2$ shell. Fig. 3e and f present high-resolution TEM images of the belt tip that is indicated in Fig. 3c. The lattice fringes yield interplanar spacings of 0.18, 0.21 and 0.25 nm of Cu (200), α-$Ni(OH)_2$ (103) and (111), respectively.

$Cu@Ni(OH)_2$ NBs are used as the electrode material in the pseudocapacitor for the following reasons. (a) The 3D web of encapsulating CuNBs provides a highly conductive network with a large surface area that promotes electron transport to the $Ni(OH)_2$ shell; (b) the thin $Ni(OH)_2$ nanosheet structure shortens ion diffusion paths and facilitates the migration of electrolyte ions at a large current density, and (c) the polymeric binder-free electrode prevents blocking of the surface soft active materials. The electrochemical properties of $Cu@Ni(OH)_2$ NBs are studied using a three-electrode system in aqueous 1 M KOH in a potential range of 0.07–0.57 V *vs.* Hg/HgO.

Fig. 4a plots the CV curves of $Cu@Ni(OH)_2$ NBs obtained at a scan rate of 5 mV s^{-1}. This figure includes a pair of redox peaks, which correspond to the $Ni(OH)_2$ redox reaction. The anodic and cathodic peaks at ~0.50 and ~0.35 V, respectively, are attributable to the reversible Faradaic redox reactions between $Ni(OH)_2$ and NiOOH (eqn (5)).

$$Ni(OH)_2 + OH^- \leftrightarrow NiOOH + H_2O + e^-. \quad (5)$$

The specific capacitance of this electrode is calculated from the CV curve to be 2608 F g^{-1}. The galvanostatic charge–discharge behavior of the electrode is studied between 0.07 and 0.57 V at a current density of 10 A g^{-1}. The nonlinear charge–discharge curves in Fig. 4b clearly reveal pseudocapacitive behavior. Additionally, the discharge curve does not exhibit an obvious *iR* drop, indicating that the electrode has low internal resistance. The specific capacitance of the $Cu@Ni(OH)_2$ NB electrode is calculated to be 2426 F g^{-1}. Fig. 4c plots the discharging curves of $Cu@Ni(OH)_2$ NBs that are obtained at current densities from 10 to 100 A g^{-1}. Fig. 4d shows the specific capacitances that are calculated from the curves shown in Fig. 4c. The $Cu@Ni(OH)_2$ NBs exhibit an excellent specific capacitance retention of 81% at a current density of 100 A g^{-1}, which is markedly higher than those obtained in previous studies on pure $Ni(OH)_2$, suggesting excellent rate capability (see Table S1 in the ESI†). The rate performance benefits from

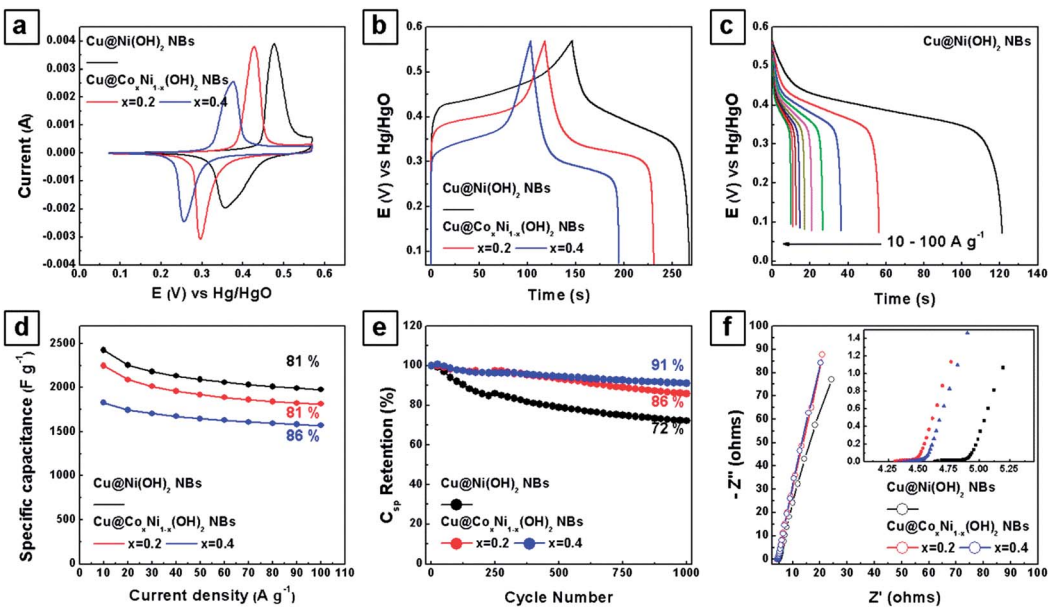

Fig. 4 (a) CV curves of $Cu@Ni(OH)_2$ NB and $Cu@Co_xNi_{1-x}(OH)_2$ NB ($x = 0.2$ and 0.4) electrodes obtained at a scan rate of 5 mV s^{-1}. (b) Galvanostatic charge–discharge curves at 10 A g^{-1} for $Cu@Ni(OH)_2$ NB and $Cu@Co_xNi_{1-x}(OH)_2$ NB electrodes. (c) Galvanostatic charge–discharge curves for the $Cu@Ni(OH)_2$ NB electrode at various current densities (10–100 A g^{-1}). (d) Corresponding specific capacitance of $Cu@Ni(OH)_2$ NB and $Cu@Co_xNi_{1-x}(OH)_2$ NB electrodes at increasing current densities. (e) Retained specific capacitance of $Cu@Ni(OH)_2$ NB and $Cu@Co_xNi_{1-x}(OH)_2$ NB electrodes as a function of the number of cycles, obtained at a scan rate of 30 A g^{-1}. (f) Comparison of Nyquist plots of electrodes made with $Cu@Ni(OH)_2$ NBs and $Cu@Co_xNi_{1-x}(OH)_2$ NBs.

the ability of the encapsulated copper NBs to support efficient electron transport and the shortening of the ion diffusion paths by the thin $Ni(OH)_2$ nanosheets.

The long-term cycling performance of the Cu@$Ni(OH)_2$ NB electrode is evaluated over 1000 galvanostatic charge–discharge cycles at 30 A g^{-1}. As shown in Fig. 4e, the fading of the capacitance (with 72% remaining) of Cu@$Ni(OH)_2$ NBs may be related to the expansion and shrinkage of the layered structures of the hydroxide by the repeated charge–discharge process.[17] However, the performance is comparable with that obtained in previous studies on pure $Ni(OH)_2$.

The enhanced electronic transport in Cu@$Ni(OH)_2$ NB electrodes is examined further by performing an electrochemical impedance spectroscopy (EIS) analysis. Fig. 4f presents the Nyquist plots of the as-prepared Cu@$Ni(OH)_2$ NB electrode that are obtained at the oxidation peak potential at frequencies from 10^5 to 10^{-1} Hz. The spectra are almost vertical at a low frequency with no semicircle at high frequency, indicating good capacitive behavior. The absence of a semicircle in the high-frequency region suggests low electrode resistance and a high rate of charge transfer between the electrolyte and the active material during the charge storage and delivery processes. Fig. S5† presents the Nyquist plot of the Cu@$Ni(OH)_2$ NB electrode after 250 cycles. The small semicircle indicates increased charge-transfer resistance, which may be the cause of the fading of the capacitance during long-term cycling.

Finally, following the literature,[17] nickel is partially substituted with cobalt (Co), which is commonly used to increase the conductivity and stability of $Ni(OH)_2$ electrodes. Fig. 4a also plots the CV curves of the Cu@$Co_xNi_{1-x}(OH)_2$ NBs ($x = 0.2$ and 0.4). The redox peak is related to the redox reactions of both cobalt and nickel hydroxide. This figure reveals no redox peak separation, indicating thorough mixing of Co–Ni binary hydroxide. The peak shifts to a lower potential as the Co content of the binary hydroxide increases. This shift in the potential of the discharge plateau is correlated closely with the CV results (Fig. 4b). The specific capacitances of these electrodes are 2250 and 1828 F g^{-1}. The Cu@$Co_{0.4}Ni_{0.6}(OH)_2$ NBs exhibit a 6% improvement rate capacitance than Cu@$Ni(OH)_2$ NBs (Fig. 4d), which is attributed to the increase in shell conductivity as the amount of conductive $Co(OH)_2$ increases relative to the amount of $Ni(OH)_2$.[17] The Cu@$Co_{0.4}Ni_{0.6}(OH)_2$ NBs also exhibit a greater capacitance retention of 91% during long-term cycling. The enhanced electrochemical properties are verified by the Nyquist plots, in which the straight line portions for Cu@$Co_xNi_{1-x}(OH)_2$ NBs ($x = 0.2$ and 0.4) are closer to the vertical spike than Cu@$Ni(OH)_2$ NBs in the low-frequency region, indicating that cobalt substitution further improves the capacitive behavior. Additionally, the effective retention of the low charge-transfer resistance of the Cu@$Co_{0.4}Ni_{0.6}(OH)_2$ NB electrode during cycling reflects the improved cyclability (Fig. S5†).

Conclusions

This work develops a cost-effective method for fabricating supercapacitors that demonstrates the feasibility of using Cu@$Ni(OH)_2$ NB electrodes for supercapacitors. Highly dense hybrid nanomaterials are prepared by aluminum-driven electrochemical deposition, which involves the galvanic deposition of CuNBs followed by coating a shell of uniform $Ni(OH)_2$ nanosheets onto the CuNB surfaces. The as-prepared electrode has a high C_{sp} of 2426 at 10 A g^{-1} and an excellent rate performance of 1977 F g^{-1}, even at 100 A g^{-1}. The electrochemical properties are enhanced by the ability of the encapsulated copper NBs to support rapid electron transport and by the shortening of ion diffusion paths by a thin $Ni(OH)_2$ nanosheet. Importantly, Cu@$Ni(OH)_2$NBs are highly promising materials for use in the next generation of high-performance supercapacitors. Moreover, the rate performance and long-term cyclic stability of these NBs can be further improved by substituting some of Ni with Co and forming the more conductive $Co(OH)_2$.

Acknowledgements

The authors would like to thank the National Science Council of the Republic of China, Taiwan, for financially supporting this research under Contract no. NSC 101-2113-M-007-012-MY3. Ted Knoy is appreciated for his editorial assistance.

Notes and references

1 J. R. Miller and P. Simon, *Science*, 2008, **321**, 651–652.
2 P. Simon and Y. Gogotsi, *Nat. Mater.*, 2008, **7**, 845–854.
3 J. Lang, X. Yan and Q. Xue, *J. Power Sources*, 2011, **196**, 7841–7846.
4 X. Lu, D. Zheng, T. Zhai, Z. Liu, Y. Huang, S. Xie and Y. Tong, *Energy Environ. Sci.*, 2011, **4**, 2915–2921.
5 Q. Lu, M. W. Lattanzi, Y. Chen, X. Kou, W. Li, X. Fan, K. M. Unruh, J. G. Chen and J. Q. Xiao, *Angew. Chem., Int. Ed.*, 2011, **50**, 6847–6850.
6 B. Saravanakumar, K. K. Purushothaman and G. Muralidharan, *ACS Appl. Mater. Interfaces*, 2012, **4**, 4484–4490.
7 Y.-L. Chen, P.-C. Chen, T.-L. Chen, C.-Y. Lee and H.-T. Chiu, *J. Mater. Chem. A*, 2013, **1**, 13301–13307.
8 K. K. Purushothaman, I. Manohara Babu, B. Sethuraman and G. Muralidharan, *ACS Appl. Mater. Interfaces*, 2013, **5**, 10767–10773.
9 T. Zhao, H. Jiang and J. Ma, *J. Power Sources*, 2011, **196**, 860–864.
10 J. W. Lee, T. Ahn, D. Soundararajan, J. M. Ko and J.-D. Kim, *Chem. Commun.*, 2011, **47**, 6305–6307.
11 J. Yan, Z. Fan, W. Sun, G. Ning, T. Wei, Q. Zhang, R. Zhang, L. Zhi and F. Wei, *Adv. Funct. Mater.*, 2012, **22**, 2632–2641.
12 J. Ji, L. L. Zhang, H. Ji, Y. Li, X. Zhao, X. Bai, X. Fan, F. Zhang and R. S. Ruoff, *ACS Nano*, 2013, **7**, 6237–6243.
13 L. Chen, L.-J. Sun, F. Luan, Y. Liang, Y. Li and X.-X. Liu, *J. Power Sources*, 2010, **195**, 3742–3747.
14 C. Meng, C. Liu, L. Chen, C. Hu and S. Fan, *Nano Lett.*, 2010, **10**, 4025–4031.
15 A. Motori, F. Sandrolini and G. Davolio, *J. Power Sources*, 1994, **48**, 361–370.

16 X. Liu, R. Ma, Y. Bando and T. Sasaki, *Adv. Mater.*, 2012, **24**, 2148–2153.
17 Y. Cheng, H. Zhang, C. V. Varanasi and J. Liu, *Energy Environ. Sci.*, 2013, **6**, 3314–3321.
18 T.-K. Huang, T.-H. Cheng, M.-Y. Yen, W.-H. Hsiao, L.-S. Wang, F.-R. Chen, J.-J. Kai, C.-Y. Lee and H.-T. Chiu, *Langmuir*, 2007, **23**, 5722–5726.
19 I. C. Chang, T.-K. Huang, H.-K. Lin, Y.-F. Tzeng, C.-W. Peng, F.-M. Pan, C.-Y. Lee and H.-T. Chiu, *ACS Appl. Mater. Interfaces*, 2009, **1**, 1375–1378.
20 A. Gutés, C. Carraro and R. Maboudian, *J. Am. Chem. Soc.*, 2010, **132**, 1476–1477.
21 I. Mintsouli, J. Georgieva, S. Armyanov, E. Valova, G. Avdeev, A. Hubin, O. Steenhaut, J. Dille, D. Tsiplakides, S. Balomenou and S. Sotiropoulos, *Appl. Catal., B*, 2013, **136–137**, 160–167.
22 L. Liu, S.-H. Yoo and S. Park, *Chem. Mater.*, 2010, **22**, 2681–2684.
23 M. Mohl, D. Dobo, A. Kukovecz, Z. Konya, K. Kordas, J. Wei, R. Vajtai and P. M. Ajayan, *J. Phys. Chem. C*, 2011, **115**, 9403–9409.
24 T. Ghodselahi, M. A. Vesaghi, A. Shafiekhani, A. Baghizadeh and M. Lameii, *Appl. Surf. Sci.*, 2008, **255**, 2730–2734.
25 C. Shang, S. Dong, S. Wang, D. Xiao, P. Han, X. Wang, L. Gu and G. Cui, *ACS Nano*, 2013, **7**, 5430–5436.